Modeling trabecular bone adaptation to local bending load regulated by mechanosensing osteocytes

Yoshitaka Kameo[a], Taiji Adachi[b]

a: Department of Mechanical Engineering, Graduate School of Engineering, Osaka Prefecture University

b: Department of Biomechanics, Research Center for Nano Medical Enginnering, Institute for Frontier Medical Sciences, Kyoto University

Corresponding author: Yoshitaka Kameo, Ph.D.

Mailing Address: Department of Mechanical Engineering

     Graduate School of Engineering

     Osaka Prefecture University

     1-1 Gakuen-cho, Naka-ku, Sakai-shi,

     Osaka 599-8531, Japan

Telephone: +81-72-254-9298

Fax: +81-72-254-9904

E-mail: kameo@me.osakafu-u.ac.jp

Abstract

Cancellous bone has a complicated three-dimensional porous microstructure that consists of strut-like or plate-like trabeculae. The arrangement of the trabeculae is remodeled throughout the organism's lifetime to functionally adapt to the surrounding mechanical environment. During bone remodeling, osteocytes buried in the bone matrix are believed to play a pivotal role as mechanosensory cells and help regulate the coupling of osteoclastic bone resorption and osteoblastic bone formation according to the mechanical stimuli. Previously, we constructed a mathematical model of trabecular bone remodeling incorporating cellular mechanosensing and intercellular signal transmission, in which osteocytes are assumed to sense the flow of interstitial fluid as a mechanical stimulus that regulates bone remodeling. Our remodeling simulation could describe the reorientation of a single strut-like trabecula under uniaxial loading. In the present study, to investigate the effects of a bending load on trabecular bone remodeling, we simulated the morphological change in a single trabecula under a cyclic bending load based on our mathematical model. The simulation results showed that the application of the bending load influences not only the formation of the plate-like trabecula but also the changes in trabecular topology. These results suggest the possibility that the characteristic trabecular morphology, such as the strut-like or plate-like form, is determined depending on the local mechanical environment.

1. Introduction

Cancellous bone has a dynamic porous structure; its density and orientation can change owing to remodeling, to adapt to the mechanical environment. The remodeling in cancellous bone takes place at the individual trabecular surface by the coupling activities of bone-resorbing osteoclasts and bone-forming osteoblasts [26]. This continuous trabecular bone remodeling results in a well-organized three-dimensional architecture of cancellous bone in the form of strut-like or plate-like trabeculae. While the importance of the mechanical environment to the maintenance of skeletal mass is widely recognized, little is known about how the mechanical signals are transduced into biochemical signals and influence the cellular activities to realize the functionally adapted bone structure.

Many experimental studies have identified that osteocytes, which are the only cell type embedded in the mineralized bone matrix, play a pivotal role in mechanosensing, and help regulate osteoclastic bone resorption and osteoblastic bone formation [5, 8, 29]. Each osteocyte is housed in a lacuna and has many slender processes extended within canaliculi, forming a three-dimensional intercellular network [20, 28]. Osteocyte processes are believed to sense the flow of surrounding interstitial fluid that is driven by the deformation of the bone matrix under dynamic loading [6, 21, 33]. In addition, recent research suggests that the ultrastructures of canaliculi have the potential to amplify the fluid-induced strain in osteocyte processes [11, 19, 32, 34].

Computational modeling is useful for investigating the quantitative relationship among the mechanical and biochemical factors involved in bone remodeling. Many remodeling models using finite element analysis have successfully predicted the structural change in bone [3, 12, 23, 30, 31]. Previously, we also proposed a mathematical model of bone remodeling that interconnects the cellular activities at the microscopic scale to the trabecular morphological changes at the macroscopic scale through the mechanical hierarchy [2, 18]. The originality of our model lies in considering the flow of interstitial fluid inside the canaliculi explicitly to be the mechanical stimulus to the osteocytes that regulate bone remodeling. The mechanical behavior of a bone matrix with lacuno-canalicular porosity is modeled as a poroelastic material [7, 15, 16] to evaluate the interstitial fluid flow under mechanical loading. Our model

was validated through a remodeling simulation for a single strut-like trabecula under physiological cyclic loading.

The individual trabecula has a characteristic morphology that is strut-like or plate-like in form depending on its position within cancellous bone. While it is certain that the morphology is associated with the mechanical environment, the determinant remains unclear. Therefore, we hypothesized that the trabecular morphology is influenced by a type of load such as a uniaxial or bending load. Our previous study demonstrated the reorientation of the strut-like trabecula under cyclic uniaxial loading [2, 18]. In the present study, we investigate the effects of a bending load on the changes in trabecular morphology. By applying our mathematical model of bone remodeling to the three-dimensional voxel finite element model of a trabecula, we performed bone remodeling simulation for a single trabecula subjected to a cyclic bending load.

2. Methods

2.1. Mathematical model of trabecular bone remodeling

Through our mathematical model, we postulate that remodeling is caused by osteoclastic bone resorption and osteoblastic bone formation on the trabecular surface, which are regulated by osteocytes responding to the interstitial fluid flow in canaliculi. In this model, the process of trabecular bone remodeling consists of three parts: (i) cellular mechanosensing, (ii) intercellular signal transmission, and (iii) trabecular surface movement due to remodeling [2, 18], as shown in Fig. 1. A summary of each process is explained below by introducing some physiologically rational assumptions.

In the cellular mechanosensing process, osteocytes were assumed to be sensitive to fluid-induced shear stress acting on their cellular processes. For evaluating the shear stress, we adopted the microstructure model of Weinbaum et al. [33] that accounts for the interstitial fluid flow through a fiber matrix in an annular canaliculus. Using the fluid pressure gradient at the trabecular level ∇p, the fluid-induced shear stress τ_p acting on the osteocyte processes aligned in direction $\boldsymbol{n}$ is given as

$$\tau_p(\boldsymbol{x},\boldsymbol{n}) = \frac{qr_p}{\gamma}\left[A_1 I_1\left(\frac{\gamma}{q}\right) - B_1 K_1\left(\frac{\gamma}{q}\right)\right]\nabla p(\boldsymbol{x})\cdot\boldsymbol{n}, \tag{1}$$

where q is the ratio of the radius of the canaliculus r_c to that of the process r_p, i.e., $q = r_c/r_p$, I_1 and K_1 are the modified Bessel functions of the first order, and the other constants are defined in Weinbaum et al. [33].

Assuming the biochemical signal that osteocytes produce in response to the fluid-induced shear stress τ_p is proportional to the shear force on their processes, the signal $S_{oc}(\boldsymbol{x})$ produced by the osteocytes per unit bone volume can be defined, by using the volume fraction of the canaliculi oriented in direction $\boldsymbol{n}$, $\rho_c(\boldsymbol{n})$, introduced in [17], as

$$S_{oc}(\boldsymbol{x}) = \int_0^{2\pi} d\varphi \int_0^{\pi/2} \alpha \frac{2r_p}{r_c^2} \rho_c(\boldsymbol{n})\overline{|\tau_p(\boldsymbol{x},\boldsymbol{n})|}\sin\theta d\theta, \tag{2}$$

where θ is the angle between the vector $\boldsymbol{n}$ and the x_3-axis in the arbitrary Cartesian coordinate system, φ is the angle between the x_1-axis and the projection of $\boldsymbol{n}$ onto the x_1x_2-plane measured counterclockwise, α is the mechanosensitivity of the osteocytes, and $\overline{|\tau_p(\boldsymbol{n})|}$ is the time-averaged shear stress over the course of 1 day. For simplicity, we set $\alpha = 1$ for all the osteocytes and assumed the isotropy of canalicular orientation, i.e., $\rho_c(\boldsymbol{n}) = \phi/2\pi$, where ϕ is the porosity of the trabeculae.

The signals produced are modeled to be transmitted to the effector cells on the trabecular surface, such as osteoclasts and osteoblasts, through the intercellular network system of bone cells. With the use of a weight function $w(l)$ that represents the decay in the signal intensity relative to the distance l, the total stimulus S_{sf} on the trabecular surface position $\boldsymbol{x}_{sf}$ is obtained in the following integral form

$$S_{sf}(\boldsymbol{x}_{sf}) = \int_\Omega w(l)S_{oc}(\boldsymbol{x})d\Omega, \quad w(l) = 1 - l/l_L \ (l \le l_L), \tag{3}$$

where $l = |\boldsymbol{x}_{sf} - \boldsymbol{x}|$. l_L denotes the maximum distance for intercellular communication and it determines the communication area Ω. The total stimulus S_{sf} is a positive scalar function and is regarded as the driving force of trabecular bone remodeling.

For modeling the self-regulation of bone mass on the trabecular surface, we introduced the empirical function that describes the relationship between the rate of trabecular surface remodeling $\dot{M}$ and the total stimulus S_{sf}, as shown in Fig. 2. In the piecewise sinusoidal function, S_{sf}^{U} is the upper threshold for bone formation, S_{sf}^{L} is the lower threshold for bone resorption, S_{sf}^{O} is a stimulus at the remodeling equilibrium, and S_{sf}^{Z} is the width of the lazy zone. This function indicates that bone resorption is initiated by stimuli below the remodeling equilibrium and bone formation is initiated by stimuli exceeding the equilibrium. To express trabecular surface movement in this simulation, the level set method [25], which is a numerical technique for tracking the interfaces and shapes of materials, was employed

2.2. Voxel finite element model of single trabecula

A three-dimensional computational model of a single trabecula for simulating the morphological changes via bone remodeling was constructed as shown in Fig. 3. The region for analysis was $a_1 \times a_2 \times a_3 = 0.8 \times 1.6 \times 1.2$ mm^3, divided into $20 \times 40 \times 30$ cubic voxel finite elements. A strut-like trabecula with a diameter of 240 μm was placed at the center of the region along the direction of the x_3-axis. The trabecula was modeled as a poroelastic material with homogeneous and isotropic material properties (Table 1) [4, 27]. To impose external loadings, two parallel plates, each with a thickness of 40 μm, were added to the upper and lower surfaces of the region for analysis. The shape of the plates does not change through the remodeling process; the plates were given the same material properties as the trabeculae.

As mechanical boundary conditions, a shear-free boundary condition was applied to the lower plate, and free leakage of interstitial fluid on the trabecular surfaces was assumed. A cyclic bending load, which was linearly distributed along the x_2 direction $\sigma = (2\sigma_3 x_2/a_2) \sin 2\pi f t$ ($f = 1$ Hz), was imposed on the upper plate in the x_3 direction for 1.0 sec per day. To investigate the effects of the magnitude of the applied bending load on the trabecular morphology, the value of σ_3 was determined as $\sigma_3 = -0.10$ and -0.15 MPa by reference to a previous remodeling simulation of cancellous bone [30]. The physiological parameters

introduced in the remodeling model are as listed in Table 2 [1, 13, 14, 35]. All the parameter settings were based on experimental findings except for the parameters associated with the mechanical stimulus— $S_{\mathrm{sf}}^{\mathrm{U}}$, $S_{\mathrm{sf}}^{\mathrm{L}}$, $S_{\mathrm{sf}}^{\mathrm{O}}$, and $S_{\mathrm{sf}}^{\mathrm{Z}}$ —which were determined arbitrarily. Among the above four parameters, $S_{\mathrm{sf}}^{\mathrm{Z}}$ representing a remodeling rate sensitivity to the stimulus near the remodeling equilibrium had a greater influence on the changes in bone volume [18]. Therefore, we performed trabecular remodeling simulations under two different settings of parameter $S_{\mathrm{sf}}^{\mathrm{Z}}$, as listed in Table 2.

3. Results

Applying the proposed mathematical model of bone remodeling to the voxel finite element model of the trabecula, we investigated the gical changes in a single trabecula subjected to an external cyclic bending load through remodeling simulations. Figs. 4 and 5 show the distribution of the 1-day average of the fluid-induced shear stress acting on the osteocyte processes $\left| \overline{\tau_{\mathrm{p}}} \right|$ at different stages of remodeling when the width of the lazy zone $S_{\mathrm{sf}}^{\mathrm{Z}}$ is equal to 0.6 μN and 0.4 μN, respectively. In both figures, part (a) corresponds to the results for the magnitude of bending load $\sigma_3 = -0.10$ MPa, and part (b) corresponds to the results for $\sigma_3 = -0.15$ MPa.

Under the loading condition $\sigma_3 = -0.10$ MPa, as shown in Fig. 4a, bone formation was promoted on all trabecular surfaces in the initial state owing to high fluid-induced shear stress. The bone formation along the x_2 direction was dominant because the applied bending load was linearly distributed along the x_2 direction. As a result, a plate-like trabecula whose dimension along the x_2 direction is larger than that along the x_1 direction was formed after 10 days. Afterward, the morphology of the trabecula was almost unchanged, while a small cavity was formed close to the upper end.

With the increase in the magnitude of the applied bending load, the fluid-induced shear stress on the trabecular surfaces increases. When $\sigma_3 = -0.15$ MPa, the remarkable bone formation for 10 days produced a plate-like trabecula with a larger width and thickness, as shown in Fig. 4b. After 20 days, unlike the case of

$\sigma_3 = -0.10$ MPa, when $\sigma_3 = -0.15$ MPa significant bone resorption occurred around the central region of the trabecula near the neutral axis of bending because the fluid-induced shear stress decreased owing to the rapid bone formation along the x_2 direction. As a result of subsequent bone resorption in the region, a branching structure was formed at the upper end of the plate-like trabecula.

A comparison of the changes in the trabecular morphology between the two different parameter settings of S_{sf}^Z, as shown in Figs. 4 and 5, shows that both remodeling processes for the first 10 days are quite similar. However, in the case of $S_{sf}^Z = 0.4$ µN, a comparatively large bone volume was lost owing to bone resorption around the central region of the plate-like trabecula. As shown in Fig. 5b, the plate-like trabecula split into two strut-like trabeculae under a large bending load.

4. Discussion

We demonstrated the morphological changes in a single trabecula under a cyclic bending load based on the remodeling model that incorporates cellular mechanosensing and intercellular signal transmission. As a result of remodeling simulations, a plate-like trabecula was formed after 10 days and the width and thickness increased with the increase in the magnitude of the bending load. The subsequent bone resorption around the central region of the trabecula contributed to forming the branching structure or split one plate-like trabecula into two strut-like trabeculae.

The trabeculae of cancellous bone *in vivo* are generally subjected to cyclic loading due to locomotion and maintenance of posture [33], which results in complex state of stress. The loading condition can be expressed as a superposition of multiple axial and bending loads in the simulation. Since the magnitude and the ratio of each load component are largely position-dependent in cancellous bone, we investigated the effects of uniaxial and bending load separately to understand the basic and primary characteristics of trabecular bone remodeling. Our previous simulation study identified the formation of a strut-like trabecula aligned along the loading direction under pure uniaxial loading [2, 18]. In contrast, the results obtained in the present remodeling simulation showed the application of the

bending load influences not only the formation of the plate-like trabecula but also the change in trabecular topology. These results suggest the possibility that the characteristic trabecular morphology, such as a strut-like or plate-like form, is determined depending on the local mechanical environment.

Whether the plate-like form is maintained for long periods depends on the magnitude of the bending load and the cellular activities at the trabecular surface. Comparing Figs. 4a with 4b shows that a large bending load causes remarkable bone loss in the neighborhood of the neutral axis of bending owing to insufficient mechanical stimuli to osteocytes. This structural change is exhibited in a trabecular remodeling simulation based on the phenomenological rule that remodeling progresses toward a locally uniform state of equivalent stress [30]. On the other hand, the decrease in the width of the remodeling lazy zone $S_{\mathrm{sf}}^{\mathrm{Z}}$ accelerated the expansion of the resorption cavity around the central region of the trabecula, as shown in Fig. 5. The lazy zone is also introduced in the mechanostat model by Frost [9, 10] as the "adaptive window" and represents the ability of the surface cells to detect changes in the local stimuli. This means that reducing the span of $S_{\mathrm{sf}}^{\mathrm{Z}}$ increases the cellular sensitivity to the mechanical stimuli. Considering the biological characteristics of the lazy zone, the simulation results can be interpreted as indicating the plate-like trabecula is likely to be formed when the cellular response is comparatively stable against the change in local mechanical stimuli.

Our remodeling model requires four parameters to describe trabecular surface movement due to remodeling, i.e., $S_{\mathrm{sf}}^{\mathrm{U}}$, $S_{\mathrm{sf}}^{\mathrm{L}}$, $S_{\mathrm{sf}}^{\mathrm{O}}$, and $S_{\mathrm{sf}}^{\mathrm{Z}}$. As reported in Kameo et al. [18], the morphological changes in the trabeculae are more sensitive to the parameter set of $S_{\mathrm{sf}}^{\mathrm{O}}$ and $S_{\mathrm{sf}}^{\mathrm{Z}}$ than to that of $S_{\mathrm{sf}}^{\mathrm{U}}$ and $S_{\mathrm{sf}}^{\mathrm{L}}$. In order to validate our results quantitatively, it is indispensable to set these empirical parameters appropriately by a comparison with experimental findings. Unfortunately, this has not been successful so far because of the difficulty of observing a single trabecula *in vivo* under a controlled mechanical condition. However, if we can reconstruct the three-dimensional trabecular bone architecture at the entire bone scale *in silico* with the aid of high-resolution scanners [22, 24], the image-based finite element analysis would help us investigate the state of stress in the region of interest and clarify the relationship between the trabecular

microstructure and the local mechanical environment. Although it cannot be quantitatively validated, our mathematical model of trabecular bone remodeling has potential for investigating how the well-organized three-dimensional architecture of cancellous bone is produced by complex metabolic activities of numerous bone cells. By incorporating the biochemical features of bone cells, such as the signaling cascade, in our remodeling model, the refined model will contribute not only to the elucidation of the mechanism of bone remodeling but also to clinical applications in the future.

Acknowledgements

References

[1] Adachi, T., Aonuma, Y., Taira, K., Hojo, M., Kamioka, H.: Asymmetric intercellular communication between bone cells: Propagation of the calcium signaling. Biochem. Biophys. Res. Commun. 389, 495-500 (2009)

[2] Adachi, T., Kameo, Y., Hojo, M.: Trabecular bone remodeling simulation considering osteocytic response to fluid-induced shear stress. Phil. Trans. R. Soc. A 368, 2669-2682 (2010)

[3] Adachi, T., Tsubota, K., Tomita, Y., Hollister, S.J.: Trabecular surface remodeling simulation for cancellous bone using microstructural voxel finite element models. J. Biomech. Eng. 123, 403-409 (2001)

[4] Beno, T., Yoon, Y.J., Cowin, S.C., Fritton, S.P.: Estimation of bone permeability using accurate microstructural measurements. J. Biomech. 39, 2378-2387 (2006)

[5] Bonewald, L.F., Johnson, M.L.: Osteocytes, mechanosensing and Wnt signaling. Bone 42, 606-615 (2008)

[6] Burger, E.H., Klein-Nulend, J.: Mechanotransduction in bone - Role of the lacuno-canalicular network. FASEB J. 13, S101-S112 (1999)

[7] Cowin, S.C.: Bone poroelasticity. J. Biomech. 32, 217-238 (1999)

[8] Cowin, S.C., Moss-Salentijn, L., Moss, M.L.: Candidates for the mechanosensory system in bone. J. Biomech. Eng. 113, 191-197 (1991)

[9] Frost, H.M.: Bone "mass" and the "mechanostat": a proposal. Anat. Rec. 219, 1-9 (1987)

[10] Frost, H.M.: Bone's mechanostat: a 2003 update. Anat. Rec. A Discov. Mol. Cell Evol. Biol. 275, 1081-1101 (2003)

[11] Han, Y., Cowin, S.C., Schaffler, M.B., Weinbaum, S.: Mechanotransduction and strain amplification in osteocyte cell processes and flow across the endothelial glycocalyx. Proc. Natl. Acad. Sci. U.S.A. 101, 16689-16694 (2004)

[12] Huiskes, R., Ruimerman, R., Van Lenthe, G.H., Janssen, J.D.: Effects of mechanical forces on maintenance and adaptation of form in trabecular bone. Nature 405, 704-706 (2000)

[13] Huo, B., Lu, X.L., Hung, C.T., Costa, K.D., Xu, Q., Whitesides, G.M., Guo, X.E.: Fluid flow induced calcium response in bone cell network. Cell. Mol. Bioeng. 1, 58-66 (2008)

[14] Jaworski, Z.F., Lok, E.: The rate of osteoclastic bone erosion in haversian remodeling sites of adult dogs rib. Calcif. Tissue Res. 10, 103-112 (1972)

[15] Kameo, Y., Adachi, T., Hojo, M.: Transient response of fluid pressure in a poroelastic material under uniaxial cyclic loading. J. Mech. Phys. Solids 56, 1794-1805 (2008)

[16] Kameo, Y., Adachi, T., Hojo, M.: Fluid pressure response in poroelastic materials subjected to cyclic loading. J. Mech. Phys. Solids 57, 1815-1827 (2009)

[17] Kameo, Y., Adachi, T., Hojo, M.: Estimation of bone permeability considering the morphology of lacuno-canalicular porosity. J. Mech. Behav. Biomed. Mater. 3, 240-248 (2010)

[18] Kameo, Y., Adachi, T., Hojo, M.: Effects of loading frequency on the functional adaptation of trabeculae predicted by bone remodeling simulation. J. Mech. Behav. Biomed. Mater. 4, 900-908 (2011)

[19] Kamioka, H., Kameo, Y., Imai, Y., Bakker, A.D., Bacabac, R.G., Yamada, N., Takaoka, A., Yamashiro, T., Adachi, T., Klein-Nulend, J.: Microscale fluid flow analysis in human osteocyte canaliculus using a realistic high-resolution image-based three-dimensional model. Integr. Biol. 4, 1198-1206 (2012)

[20] Kamioka, H., Honjo, T., Takano-Yamamoto T.: A three-dimensional distribution of osteocyte processes revealed by the combination of confocal laser scanning microscopy and differential interface contrast microscopy. Bone 28, 145-149 (2001)

[21] Knothe Tate, M.L., Knothe, U., Niederer, P.: Experimental elucidation of mechanical load-induced fluid flow and its potential role in bone metabolism and functional adaptation. Am. J. Med. Sci. 316, 189-195 (1998)

[22] Majumdar, S., Kothari, M., Augat, P., Newitt, D.C., Link, T.M., Lin, J.C., Lang, T., Lu, Y., Genant. H.K.: High-resolution magnetic resonance imaging: three-dimensional trabecular bone architecture and biomechanical properties. Bone 22, 445-454 (1998)

[23]McNamara, L.M., Prendergast, P.J.: Bone remodelling algorithms incorporating both strain and microdamage stimuli. J. Biomech. 40, 1381-1391 (2007)

[24]Müller, R., Hildebrand, T., Rüegsegger, P.: Non-invasive bone biopsy: a new method to analyse and display the three-dimensional structure of trabecular bone. Phys. Med. Biol. 39, 145-164 (1994)

[25]Osher, S., Sethian, J.A.: Fronts propagating with curvature-dependent speed: algorithms based on Hamilton-Jacobi formulation. J. Comput. Phys. 79, 12-49 (1988)

[26]Parfitt, A.M.: Osteonal and hemi-osteonal remodeling: The spatial and temporal framework for signal traffic in adult human bone. J. Cell. Biochem. 55, 273-286 (1994)

[27]Smit, T.H., Huyghe, J.M., Cowin, S.C.: Estimation of the poroelastic parameters of cortical bone. J. Biomech. 35, 829-835 (2002)

[28]Sugawara, Y., Kamioka, H., Honjo, T., Tezuka, K., Takano-Yamamoto, T.: Three-dimensional reconstruction of chick calvarial osteocytes and their cell processes using confocal microscopy. Bone 36, 877-883 (2005)

[29]Tatsumi, S., Ishii, K., Amizuka, N., Li, M.Q., Kobayashi, T., Kohno, K., Ito, M., Takeshita, S., Ikeda, K.: Targeted ablation of osteocytes induces osteoporosis with defective mechanotransduction. Cell Metab. 5, 464-475 (2007)

[30]Tsubota, K., Adachi, T.: Spatial and temporal regulation of cancellous bone structure: Characterization of a rate equation of trabecular surface remodeling. Med. Eng. Phys. 27, 305-311 (2005)

[31]Tsubota, K., Suzuki, Y., Yamada, T., Hojo, M., Makinouchi, A., Adachi, T.: Computer simulation of trabecular remodeling in human proximal femur using large-scale voxel FE models: Approach to understanding Wolff's law. J. Biomech. 42, 1088-1094 (2009)

[32]Wang, Y., McNamara, L.M., Schaffler, M.B., Weinbaum, S.: A model for the role of integrins in flow induced mechanotransduction in osteocytes. Proc. Natl. Acad. Sci. U.S.A. 104, 15941-15946 (2007)

[33]Weinbaum, S., Cowin, S.C., Zeng, Y.: A model for the excitation of osteocytes by mechanical loading-induced bone fluid shear stresses. J. Biomech. 27, 339-360 (1994)

[34] You, L.D., Cowin, S.C., Schaffler, M.B., Weinbaum, S.: A model for strain amplification in the actin cytoskeleton of osteocytes due to fluid drag on pericellular matrix. J. Biomech. 34, 1375-1386 (2001)

[35] You, L.D., Weinbaum, S., Cowin S.C., Schaffler M.B.: Ultrastructure of the osteocyte process and its pericellular matrix. Anat. Rec. A 278A, 505-513 (2004)
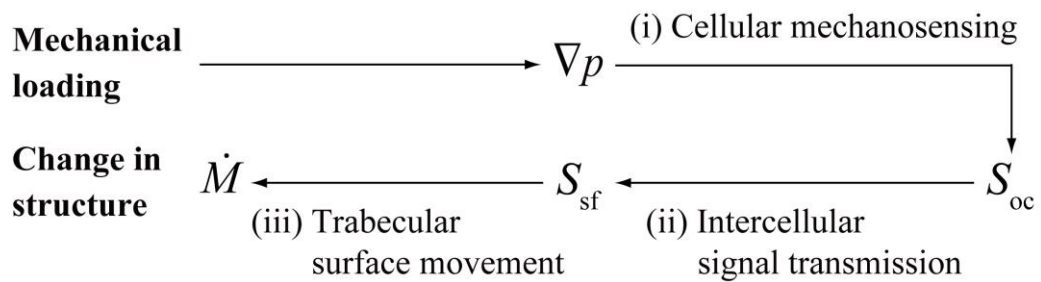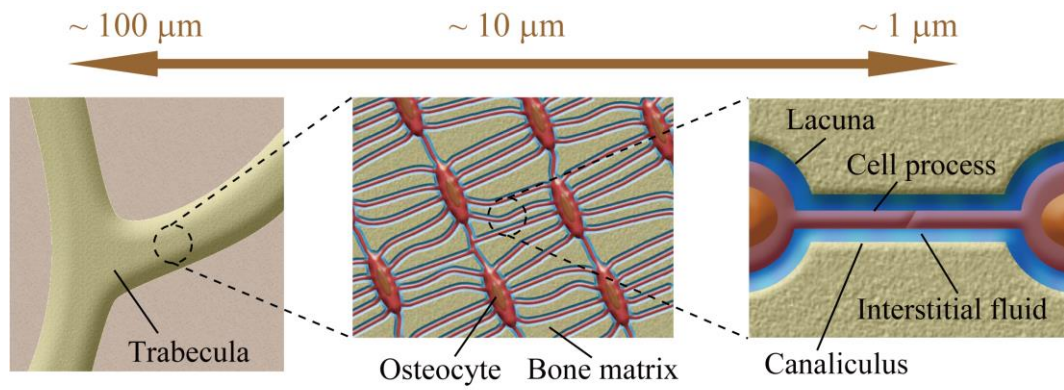
Fig. 1 Theoretical framework for trabecular bone remodeling considering the mechanical hierarchy from the microscopic level (~ 1 μm) to the macroscopic level (~ 100 μm). The remodeling process consists of the following three parts: (i) cellular mechanosensing, (ii) intercellular signal transmission, and (iii) trabecular surface movement. The change in trabecular structure is caused by osteoclastic bone resorption and osteoblastic bone formation. Their metabolic activities are regulated by osteocytes in response to the interstitial fluid flow in canaliculi.
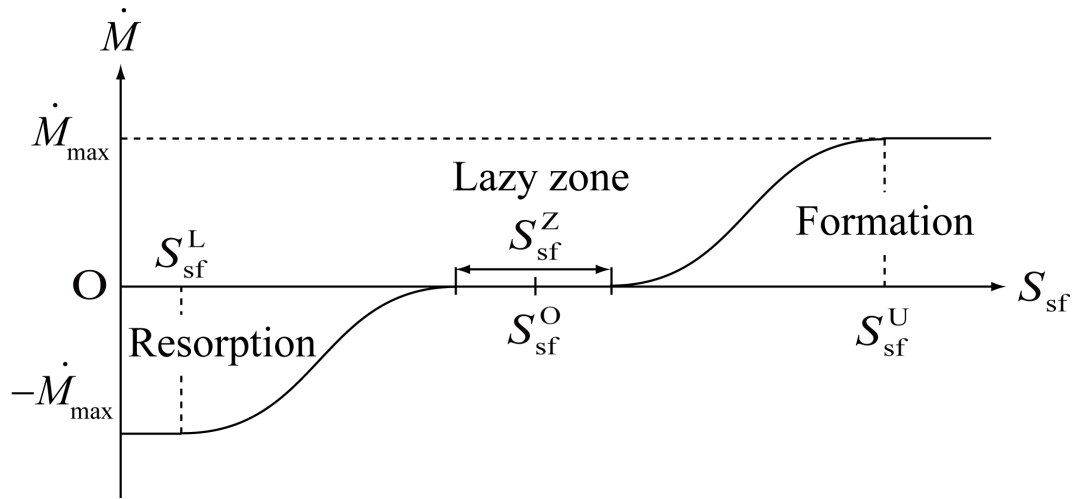
Fig. 2 Relationship between the rate of trabecular surface remodeling $\dot{M}$ and the total stimulus S_{sf} that the trabecular surface cell receives from the neighboring osteocytes. This relationship is assumed to be represented by a piecewise sinusoidal function.
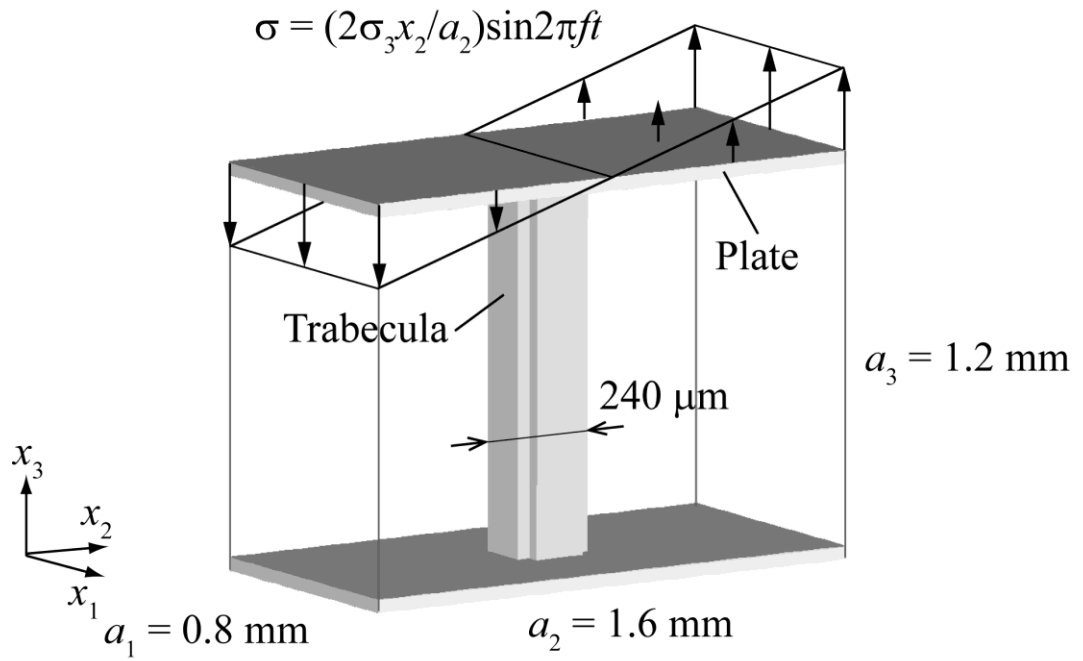
Fig. 3 Voxel finite element model of a single trabecula with a diameter of 240 μm. A cyclic bending load, which was linearly distributed along the x_2 direction, was applied on the upper plane along the x_3 direction for 1.0 sec per day.
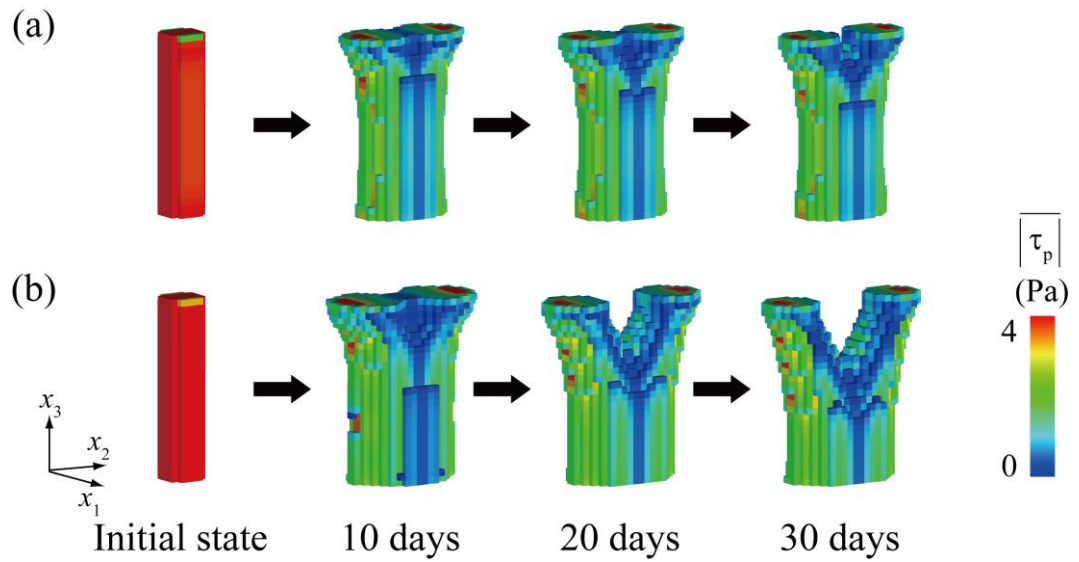
Fig. 4 Changes in the trabecular morphology and average fluid-induced shear stresses in 1 day $\overline{|\tau_{\mathrm{p}}|}$ under a cyclic bending load when the width of the lazy zone $S_{\mathrm{sf}}^{\mathrm{Z}}$ is 0.6 μN: (a) $\sigma_3 = -0.10$ MPa and (b) $\sigma_3 = -0.15$ MPa.
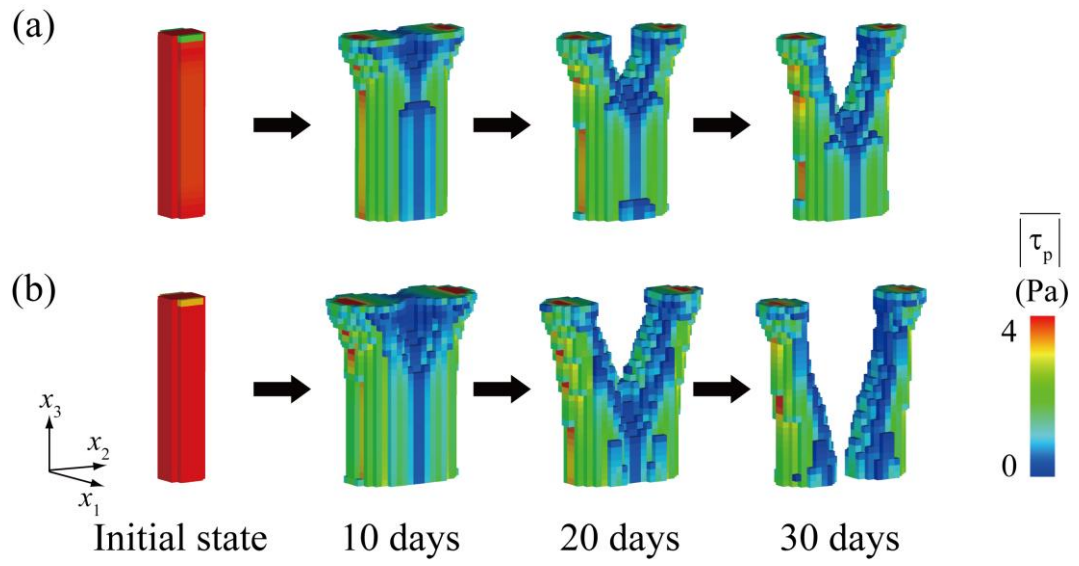
Fig. 5 Changes in the trabecular morphology and average fluid-induced shear stresses in 1 day $\overline{|\tau_\mathrm{p}|}$ under a cyclic bending load when the width of the lazy zone S_sf^Z is 0.4 μN: (a) $\sigma_3 = -0.10$ MPa and (b) $\sigma_3 = -0.15$ MPa.

Table 1 Material properties of the trabecula as a poroelastic material [4, 27]

Symbol (unit)	Description	Value
k (m²)	Intrinsic permeability	1.1×10^{-21}
μ (Pa·s)	Fluid viscosity	1.0×10^{-3}
G (GPa)	Shear modulus	5.94
ν	Drained Poissons's ratio	0.325
K_s (GPa)	Solid bulk modulus	17.66
K_f (GPa)	Fluid bulk modulus	2.3
ϕ	Porosity	0.05

Permeability was estimated by the method of Beno et al. (2006).
The other constants were taken from Smit et al. (2002).

Table 2   Parameter settings for the trabecular remodeling simulation [1, 13, 14, 35]

Symbol (unit)	Description	Value
r_p (nm)	Radius of osteocyte process	52[a]
r_c (nm)	Radius of canaliculus	129.5[a]
$\dot{M}_{max}$ (μm/day)	Maximum remodeling rate	40[b]
l_L (μm)	Maximum distance for intercellular communication	200[c,d]
S_{sf}^{U} (μN)	Upper threshold for bone formation	1.0
S_{sf}^{L} (μN)	Lower threshold for bone resorption	13
S_{sf}^{O} (μN)	Stimulus at remodeling equilibrium	7.0
S_{sf}^{Z} (μN)	Width of lazy zone	0.6 or 0.4

[a] You et al. (2004)
[b] Jaworski and Lok (1972)
[c] Huo et al. (2008)
[d] Adachi et al. (2009)